

Measurement of Slip-Band Size of α -Brass in Fatigue by Means of Scanning Atomic-Force Microscopy

Yoshikazu NAKAI, Dept. of Mech. Eng., Kobe University, Nada, Kobe 657-8501, Japan
Teppeï KUSUKAWA, Graduate School, Kobe University, Nada, Kobe 657-8501, Japan
Naohiko HAYASHI, Minolta Co., Ltd., Chuo, Osaka 541-8556, Japan

Since the surface morphology of materials can be observed with atomic-scale resolution, scanning atomic force microscopy (AFM) is a powerful technique to study mechanisms of fatigue and fracture of solid materials. In the present study, slip-band formation and fatigue crack-initiation processes in α -brass were observed by means of AFM. Although the slip-band angle relative to the stress-axis at the specimen surface varies from 15 to 90°, it took peak value at 60°. The depth of the intrusion drastically increased with its outgrowth to a crack, and with coalescence of cracks, the width of cracks increased rapidly. Before crack-initiation, the upper limit of the intrusion depth is given as a function of the slip-band angle by a geometrical model for the slip-direction and the slip-step. Slip-bands have steep slope when they are blocked by grain boundaries, and the slip-bands descend by gradual slopes to plain surfaces when they terminate within grains.

Key Words: Fatigue, micromechanics, crack-initiation, slip-band, α -brass, AFM

1. Introduction

It is well known that the fatigue process of metallic materials without macroscopic defects can be divided into initiation and growth processes of cracks and final unstable fracture. Among these processes, various studies have been conducted on crack-growth behavior, and that can be quantitatively analyzed based on fracture mechanics [1-3].

Most studies on mechanisms of the metal fatigue have been conducted with optical microscopes and electron microscopes. With these conventional microscopes, however, continuous quantitative three-dimensional observations of the crack nucleation portion in the specimen surface could not be conducted, although many studies have been done about intrusions and extrusions in fatigue slip-bands [4-8]. In most of these studies, the crack-initiation mechanisms were discussed qualitatively. The initiation condition of fatigue micro-cracks, however, still has not clarified enough, because no method for continuous direct and quantitative observation of the process has been devised. For example, precise observations of the structures of fatigue slip-bands have been conducted with the transmission electron microscope. This method, however, requires cutting of the specimen. Thus continuous observation for a specific slip-band could not be achieved. The X-ray micro-beam provided crystallographic information during fatigue process [9], but geometrical information could not be obtained from it.

Since the surface morphology of materials can be observed with atomic-scale resolution, the scanning atomic force microscopy (AFM) is a powerful technique to study mechanisms of fatigue and fracture of solid materials. By using AFM, Komai et al. observed the micro-crack-initiation and growth behavior in stress corrosion cracking [10]. Matsuoka et al. observed cleavage fracture surface [11]. For fatigue micro-mechanisms, Choi et al. examined fatigue striation shape [12]. Yoon et al. observed the nucleation mechanism of intergranular cracks in high-cycle fatigue [13]. Ohgi et al. observed crack-initiation at grain boundaries in low-cycle fatigue [14]. Nakai et al. have studied fatigue slip-bands, fatigue crack-initiation, and the growth behavior of micro-cracks in a structural steel

[15].

In our previous study with α -brass, slip-band formation and fatigue crack-initiation processes were observed by means of AFM [16, 17]. Surface of a fatigued specimen was observed at maximum stress, unloading state, and minimum stress in fatigue loading. In the initial stage of the fatigue process, slip-bands which were formed only under tension stress or compression stress were observed. These kinds of slip-bands, however, disappeared shortly. Under tension stress, cracks could be detected easily just after initiation from the AFM image. Before crack-initiation, the height and the width of extrusions and depth and width of intrusions gradually increased with the number of cycles. When extrusions developed cracks, one of these values changed drastically, depending on the slip-band angle relative to the stress-axis and the shape of slip-bands.

In the present study, slip-band formation and fatigue crack-initiation processes in α -brass were observed by means of AFM and the conditions for crack-initiation was discussed as a function of slip-band angle. The shape of slip-bands also observed and discussed based on the continuum distributed dislocation theory.

2. Theory

2.1 Angle of Slip-Band Relative to Stress-Axis

Figure 1 (a) explains the relation between surface-step and slip-direction, where the cube ABCDEFGO indicates a small region of a specimen that is located adjacent to the surface [1, 18]. In the figure, plane ABCD represents the specimen surface, plane CKLM represents the slip plane, and y-axis and arrow QH represents the loading-direction. Line CK is the slip trace at the specimen surface and line ST is on the slip plane and parallel to line KC. Arrow HR is the slip-direction on the slip-plane, and arrow HP is the normal of the slip-plane. The surface-step induced by the slip is

$$d = s \cdot \sin\beta \cdot \cos\alpha' \quad (1)$$

where s is the slip distance in the HR direction, α' is the angle between the normal to the surface and the trace of the slip-band on the plane that is perpendicular to the surface and parallel to the loading-axis, and β is the angle between the slip-direction and the slip-traces on

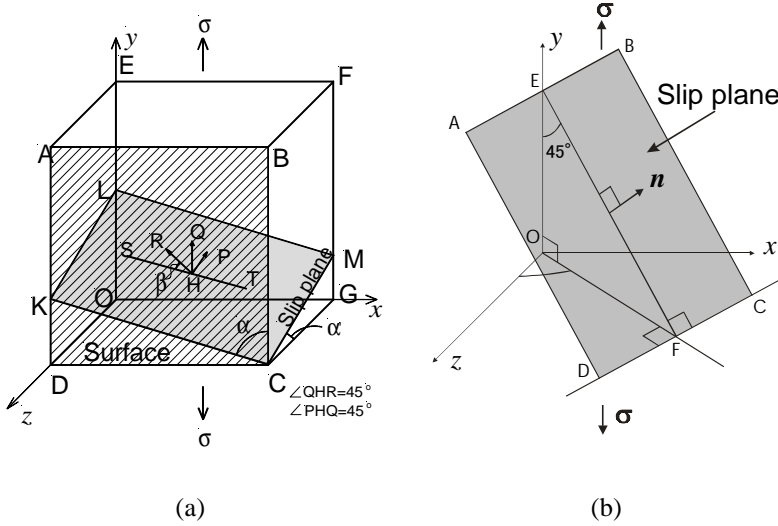


Fig. 1. Slip-plane and directions relative to stress-axis and surface.

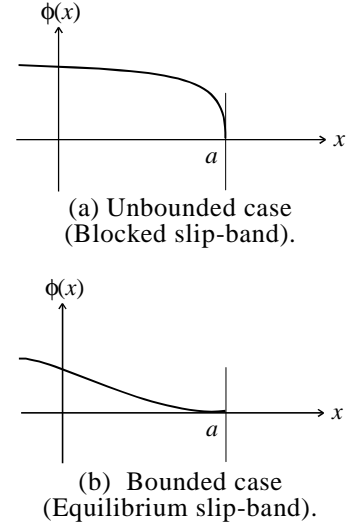


Fig. 2. Relative displacement induced by continuum distributed dislocations.

the surface (see Fig. 1 (a)). When $\angle QHR = \angle PHQ = 45^\circ$, the resolved shear stress along the slip-direction take the maximum value, and the following relation should be satisfied.

$$\cos \beta = \sqrt{2} \cos \alpha \quad (2)$$

For $\alpha=90^\circ$, the value of β should be 90° , which gives the maximum roughness of the surface for a given slip distance. For $\alpha = 45^\circ$, the value of β should be 0° and no slip step forms on the specimen surface.

Along the slip plane where the resolved shear stress takes the maximum value, the following equation should be satisfied.

$$\cot^2 \alpha + \tan^2 \alpha' = 1 \quad (3)$$

The direction of slip-plane relative to the specimen surface also can be characterized by the angle ϕ shown in Fig. 1 (b), and the value of ϕ is calculated from the angle α as

$$\sin \phi = \frac{1}{\tan \alpha} \quad (4)$$

where ϕ is the angle between surface normal and projection of the normal of slip-plane on x - z plane.

2.2 Blocked Slip-Band and Equilibrium Slip-Band

By the theory of continuum distributed dislocations, the relative displacement induced by infinitesimal dislocations, $\phi(x)$, is given by

$$\phi(x) = \int D(\xi) d\xi \quad (5)$$

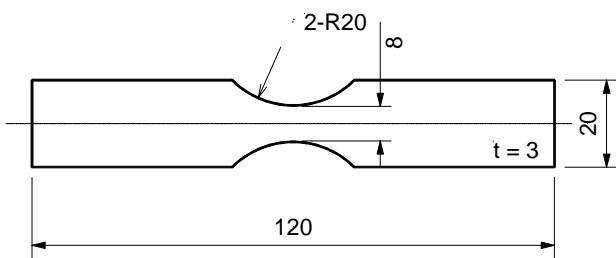


Fig. 3. Shape and dimensions of specimen (in mm).

where $D(\xi)$ is the dislocation density. Muskhelishvili has given explicitly the formulas for $D(x)$, which has different form depending whether $D(x)$ is to be bounded or unbounded at the endpoints [19]. The relative displacement for each case is schematically shown in Fig. 2 [20].

For a slip-band, whose endpoint is blocked by a grain-boundary, the dislocation density, $D(\xi)$ at the point ($x=a$) is unbounded, and the value of $D(a)$ is vanished for an equilibrium slip-band which is terminated within a grain [21].

3. Experimental Procedure

The material for the present study was α -brass (70-30 brass). The chemical composition of the material (in mass %) is as follows: 69.92 Cu, 30.07 Zn, 0.0071 Fe, and 0.0026 Pb. The material was heat treated at 320°C for 180 s after the specimens were made by electric-discharge machining. The yield strength was 217 MPa, the tensile strength was 363 MPa, and the elongation was 54 % after heat treatment. Before fatigue tests, the surface of the specimens was electro-chemically polished. As shown in Fig. 3, the specimen has a minimum cross-section of width 8 mm and thickness 3 mm, and has a weak stress concentration with the elastic stress concentration factor 1.03 under plane bending [22].

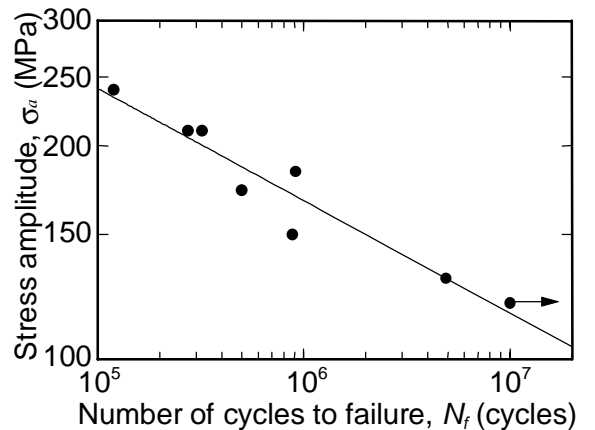


Fig. 4. S-N curve.

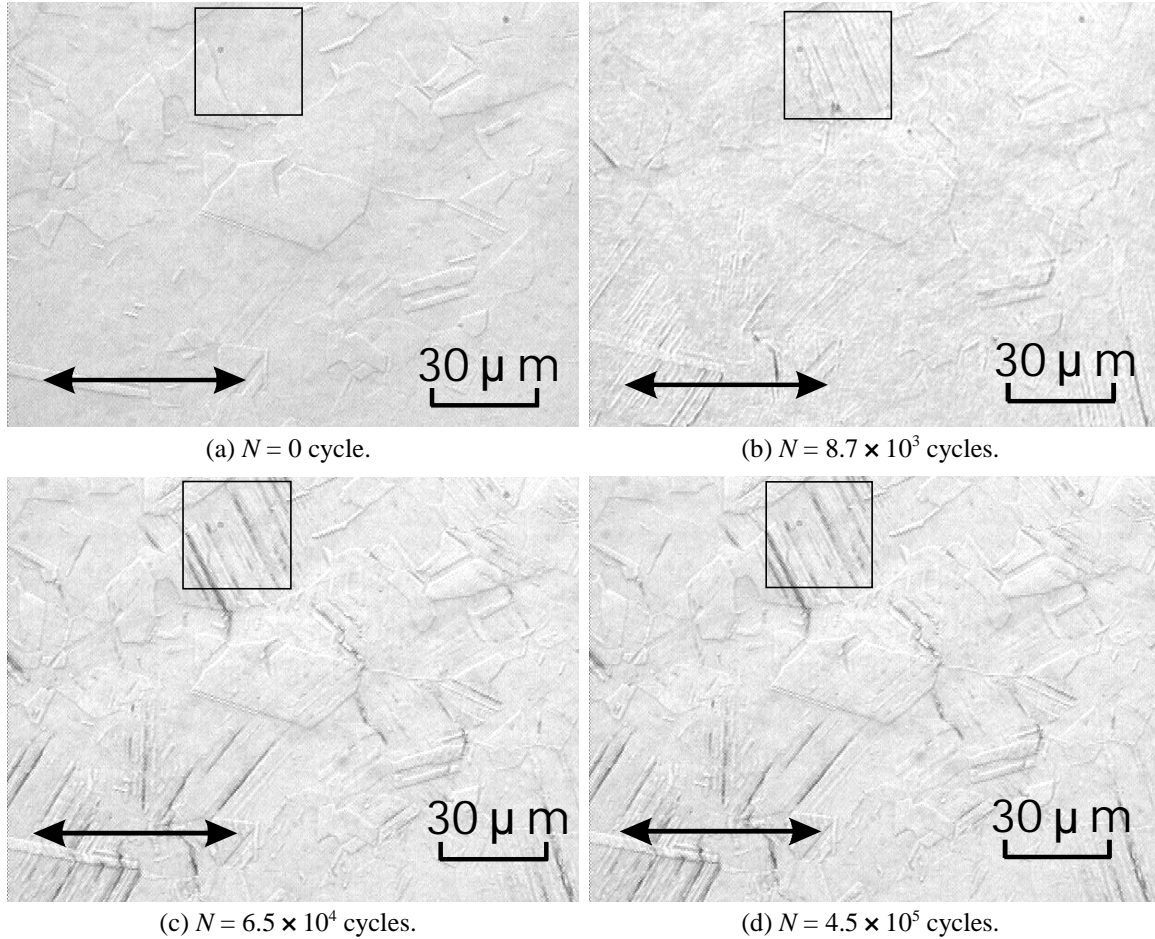


Fig. 5. Optical micrographs of fatigue slip-bands.

The fatigue tests were carried out in a computer-controlled electro-dynamic vibrator operated at a frequency of 30 Hz under fully reversed cyclic plane bending moment ($R = -1$). Since it was very difficult to identify in advance where fatigue cracks would nucleate, we took replicas at the predetermined number of fatigue cycles. The replica films were coated by Au before observation. The replications were conducted at maximum tensile stress. Although the height of the surface is reversed from the original surface by the replication method, the height of the replica film in the AFM images was reversed by an image processing technique.

As shown in Fig. 4, the fatigue strength of the present material for 10^7 cycles is about 130 MPa. The observation of the fatigue process with AFM was conducted at a stress amplitude, σ_a , of 173 MPa. The number of cycles to failure at this stress amplitude was 5.0×10^5 .

4. Experimental Results and Discussion

4.1 Optical Microscopy of Slip-Bands

Optical micrographs of fatigue crack-initiation process are shown in Fig. 5, where arrows indicate loading-direction. To examine the slip-direction, the surface slip-direction relative to the stress-axis is shown in Fig. 6 (a). The total number of slip-bands to be examined was 325. The probability was defined as the number of slip-bands observed for each angle interval divided by the total number of slip-bands examined. The results show that the slip plane is not exactly on the maximum shear stress plane because the slip-band angle

at the specimen surface less than 45° is observed. For the angle larger than 45° , the slip appearance probability is not constant. It takes maximum value at the angle $\alpha = 60^\circ$. One possible origin for this angle dependence is that the angle ϕ , which is defined in Fig. 1 (b), may be randomly distributed, but the angle α , which is defined in Fig. 1 (a), is not linear with the angle, ϕ . To compensate this non-linearity, the number of slip-bands at each angle interval was modified as

$$n' = n \cdot \frac{\Delta\alpha}{\Delta\phi} \quad (6)$$

The modified probability, which was calculated from n' , is shown in Fig. 6 (b), where $\Delta\alpha$ was 5° , and $\Delta\phi$ was calculated from Eq. (4). Since the value of ϕ in Eq. (4) can be obtained for the value of α greater than 45° , the modified probability was calculated only for $\alpha > 45^\circ$. The modified probability also takes peak value at 60° . The constraint from adjacent grains and the surface energy to produce slip-step at the specimen surface may be considered in the distribution of the slip-angle.

4.2 Development of Slip-Bands and Crack Initiation

Although the direction of slip-bands can be measured, the surface geometry of slip-bands could not clarified from the optical micrographs. To conduct quantitative analysis for the development of fatigue slip-bands, the scanning atomic force microscopy (AFM) was employed for the present study. The scanning area for these AFM observations in this section was $30 \mu\text{m} \times 30 \mu\text{m}$.

AFM images of slip-bands, which are surrounded by solid lines in Fig. 5, are shown in Fig. 7 where arrows indicate the loading-direction. In these figures, shade indicates the height of the specimen surface, *i.e.*, darker indicates lower, and lighter shows higher. It is clear from AFM images that two parallel fatigue cracks were formed at $N=9.1 \times 10^4$ cycles (Fig. 6 (d)), and they were coalesced at $N=4.5 \times 10^5$ cycles. From the corresponding optical micrographs shown in Fig. 5, it is impossible to distinguish between slip bands and cracks.

The change of geometry of cross section A, which is indicated in Fig. 7 (a), is shown in Fig. 8. With the crack-initiation at $N=9.1 \times 10^4$ cycles, the depth of intrusion increased rapidly, and with coalescence of cracks at $N=4.5 \times 10^5$ cycles, the width of the cracks increased rapidly.

Change of the intrusion depth is shown in Fig. 9 as a function of the number of the fatigue cycles, N . The depth of the intrusion drastically increased with its

outgrowth to a crack at $N = 9.1 \times 10^4$ cycles.

To examine the critical value of the intrusion depth for crack-initiation, the depth of intrusion is plotted in Fig. 10 as a function of the intrusion angle relative to the stress-axis. At $N=2.4 \times 10^4$ (Fig. 10 (a)), no crack were formed, but cracks were already initiated at $N=4.5 \times 10^4$ (Fig. 10 (b)). The solid-line in these figures shows the relationship, given through Eqs. (1) to (3). For slip-bands, the theory gives upper limit of their depth, *i.e.*, all data falls below the solid line. On the other hand, the theory does not give the intrusion depth after crack-initiation.

4.3 Shape of Slip-Band Tip

The morphology of endpoints of slip-bands was observed with higher magnification, and they were compared with the results, which were predicted from the continuum distributed dislocation theory. Figure

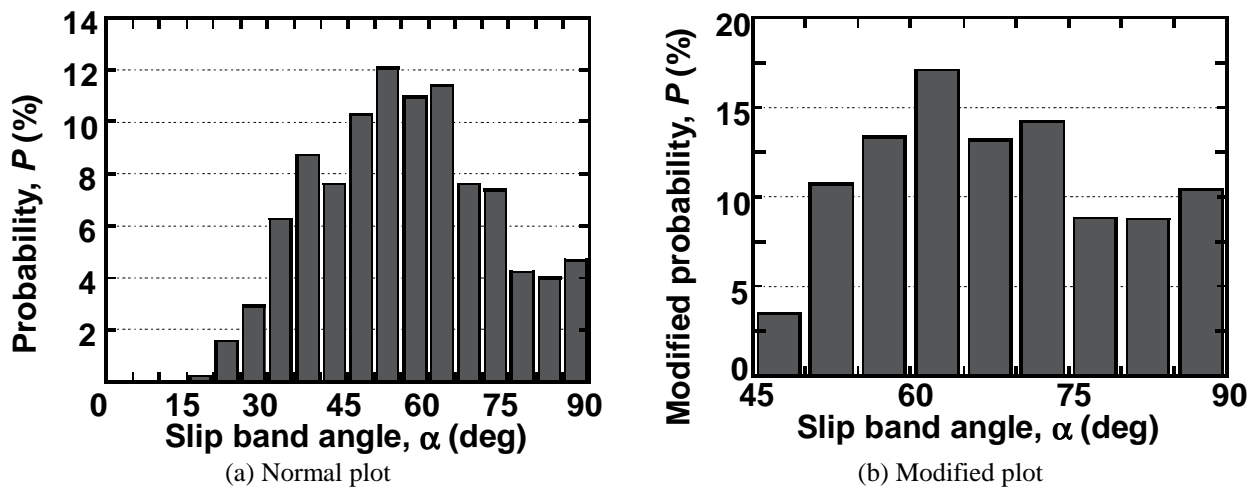


Fig. 6. Angular distribution of slip-bands.

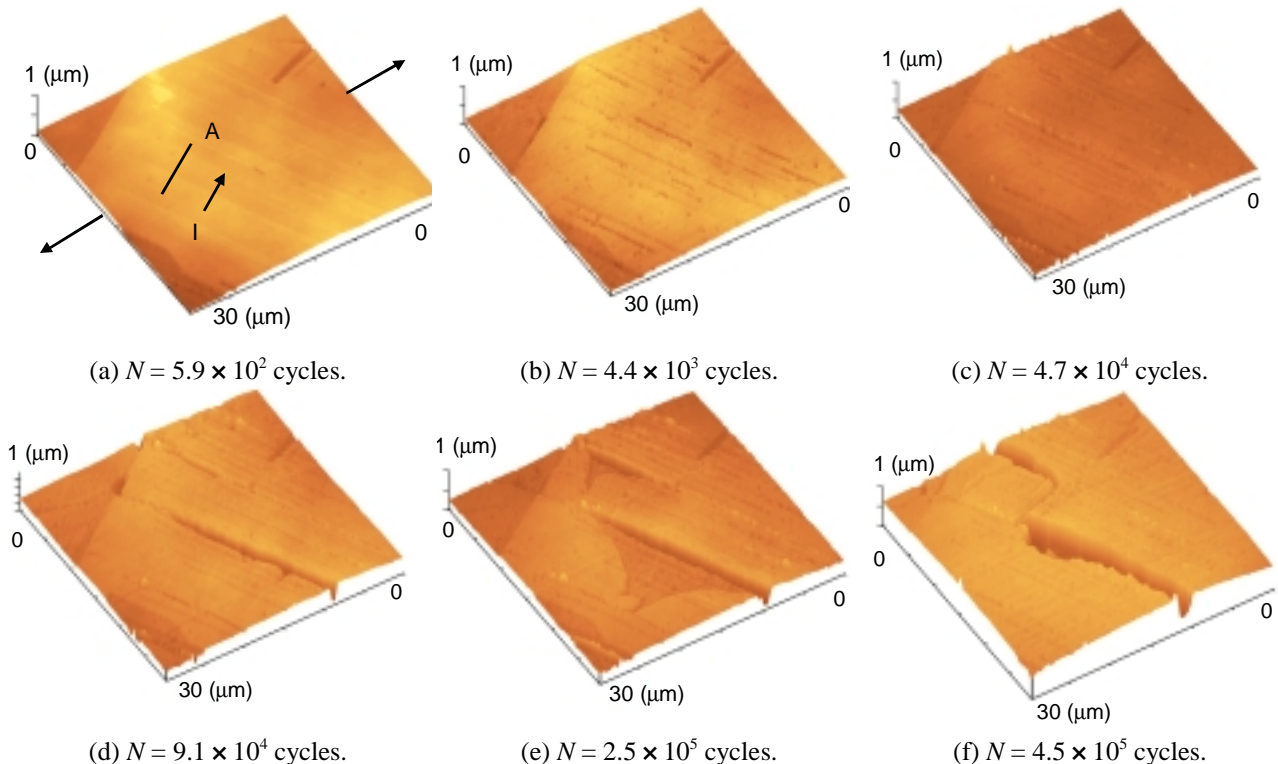


Fig. 7. AFM images in fatigue crack-initiation process.

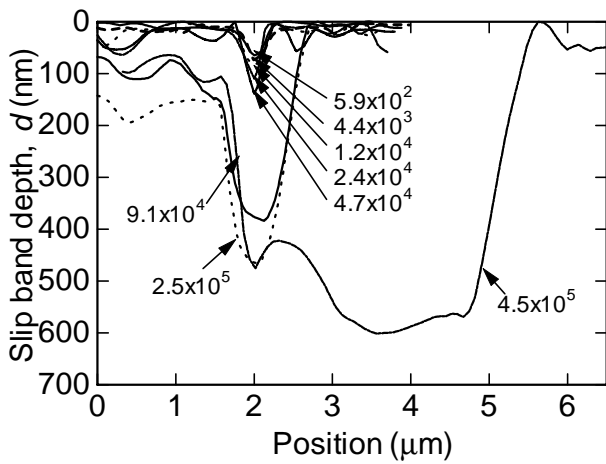


Fig. 8. Change of intrusion geometry in fatigue.

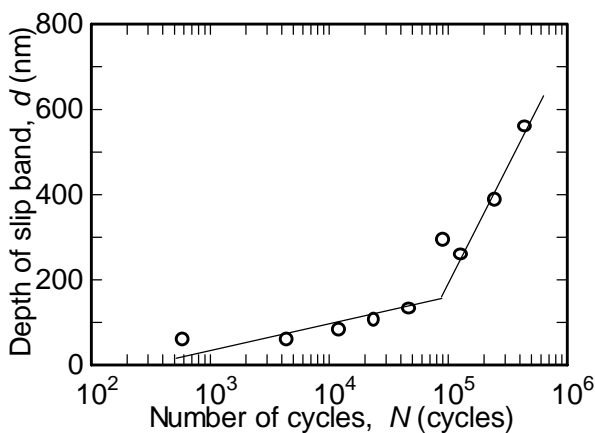


Fig. 9. Growth of intrusion in fatigue.

11 shows some examples of endpoints of slip-bands, and Figure 12 indicates profiles of peaks of extrusions or valleys of intrusions near their endpoints, where “*blocked slip-band*” means that it terminates at a grain boundary, and “*equilibrium slip-band*” means that it ends within a grain. It is clear from these figures that slip-bands have steep slope when they are blocked by grain boundaries, and the slip-bands descend by gradual slopes to plain surfaces when they end within grains. These observations are consistent with the results predicted from the continuum distributed dislocation theory.

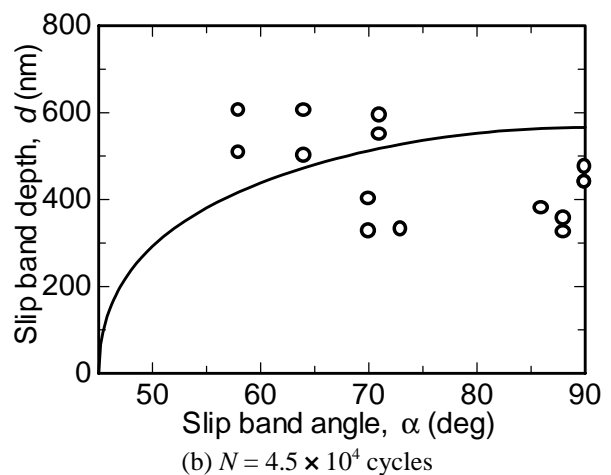
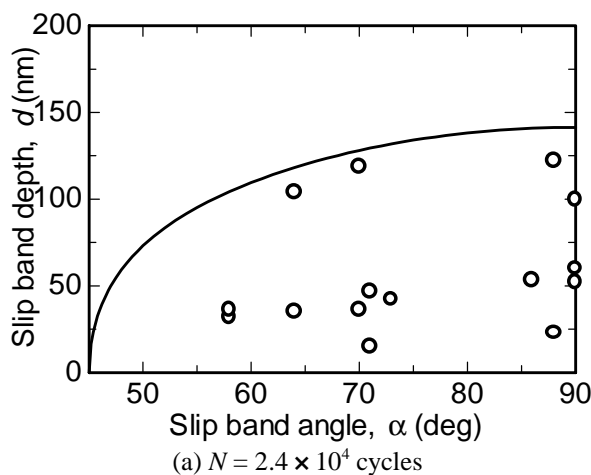


Fig. 10. Slip band angle relative to stress-axis.

4. Conclusions

The fatigue slip-band formation and fatigue crack-initiation process in α -brass were observed by means of optical microscopy and scanning atomic force microscopy (AFM). The following results were obtained.

- (1) The slip-band angle relative to the stress-axis at the specimen surface took peak value at 60° .
- (2) The depth of the intrusion drastically increased with its outgrowth to a crack, and with coalescence of cracks, the width of cracks increased rapidly.
- (3) Before crack-initiation, the upper limit of the intrusion depth is given as a function of slip-band angle by applying a geometrical model for the slip-direction and the slip-step.
- (4) Slip-bands have steep slope when they are blocked by grain boundaries, and the slip-bands descend by gradual slopes to plain-surfaces when they end within grains.

Acknowledgment

Support of this work by Grant-in-Aid for Scientific Research (C) (Project No. 10650090) by Japanese Ministry of Education, Science, Sports and Culture is gratefully acknowledged.

5. References

1. Tanaka, K., Hojo, M., and Nakai, Y., ASTM STP 811 (1983), pp. 207-232.
2. Nakai, Y. and Tanaka, K., Proc. 23rd Japan Cong. Mat. Res. (1980), pp.106-112.
3. Nakai, Y., Tanaka, K., and Yamashita, Int. J. Fract., **17** (1981), pp.519-533.
4. M., Takao, K. and Nisitani, H., Trans. JSME, **46** (1980), pp. 123-130.
5. Ma, B.,T. and Laird, C. Small Fatigue Cracks (1986), pp. 9-28, Ritchie, R. O., and Lankford, J. (Ed.), The Metallurgical Society, Inc., Warrendale, Pennsylvania.
6. Fine, M. E. and Kwon, I. B., Small Fatigue Cracks (1986), pp. 29-40, Ritchie, R. O., and Lankford, J. (Ed.), The Metallurgical Society, Inc., Warrendale, Pennsylvania.
7. Neumann, P., Tönnessen, A., Small Fatigue Cracks (1986), pp. 41-47, Ritchie, R. O., and Lankford, J. (Ed.), The Metallurgical Society, Inc., Warrendale, Pennsylvania.
8. Bayerlein, M. and Mughrabi, H. (1992), ESIS 13, pp. 55-82.
9. Taira, S., Hayashi, K., and Tanaka, K., J. Mat. Sci., Japan, **15** (1966), pp. 879-886.
10. Komai, K., Minoshima, K., and Itoh, M., J. Mat. Sci., Japan, **43** (1994), pp. 336-342.
11. Matsuoka, S., Sumiyoshi, H., Ishikawa, K., Trans. Japan Soc. Mech. Eng., **56A** (1990), pp. 2091-2097.

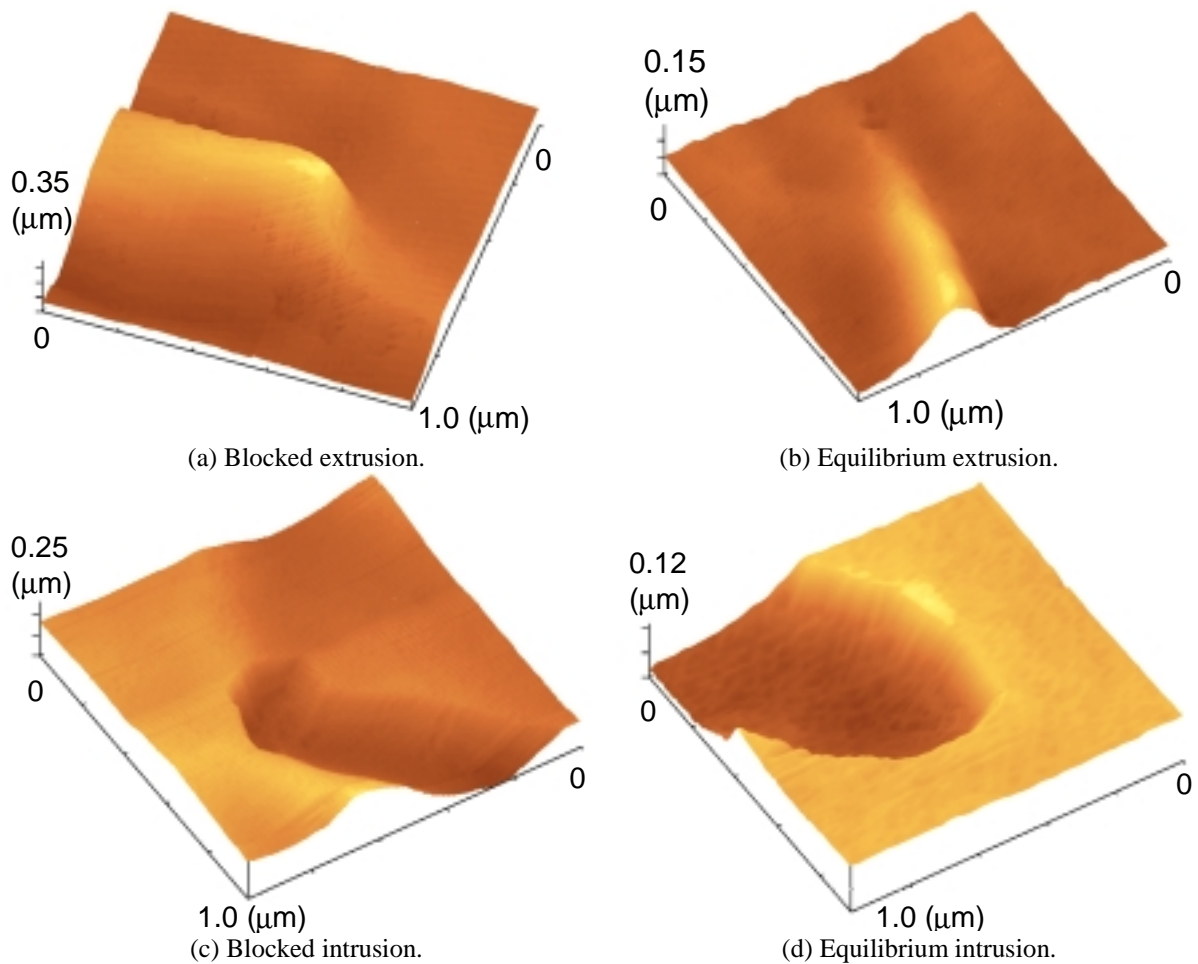


Fig. 11. Surface geometry around slip-band tips.

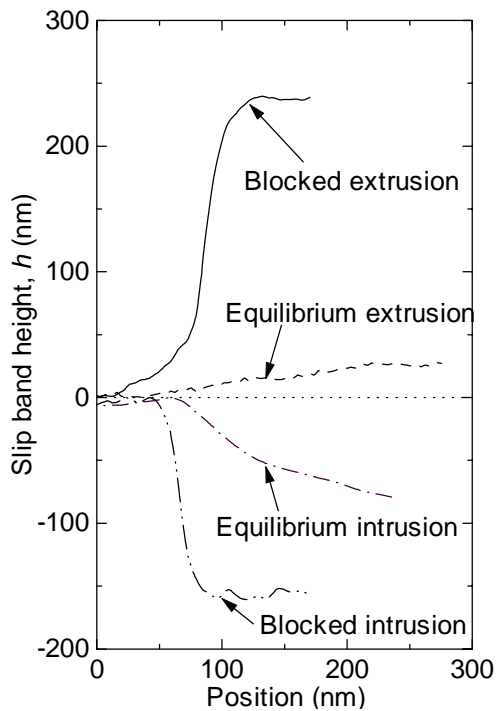


Fig. 12. Height of surface at the ends of slip-bands

12. Choi, S., Ishii, H., S., and Tohgo, K., *J. Mat. Sci., Japan*, **47** (1998), pp. 852-857.
13. Yoon, W. K., Inoue T., Noguchi, H., and Higashida, K., *Trans. JSME*, **64A** (1998), pp. 1435-1442.
14. Ohgi, J., Hatanaka, K., and Zenge, T., *Proc. 1998 Annual Meeting of JSME/MMD* (1998), pp207-208.
15. Nakai, Y., Fukuhara, S., and Ohnishi, K., *Int. J. Fatigue*, **19S** (1997), pp. 223-236.
16. Nakai, Y., Ohnishi, K., and Kusukawa, T., *Trans. Japan Soc. Mech. Eng.*, **65A** (1999), pp. 483-490.
17. Nakai, Y., Ohnishi, K., and Kusukawa, T., To be published in *Small Fatigue Cracks: Mechanics and Mechanisms*, Elsevier Science (1999).
18. Tanaka, K., Nakai, Y., and Maekawa, O., *J. Soc. Mat. Sci., Japan*, **31** (1982), pp. 376-382.
19. Taira, S., Tanaka, K., and Nakai, Y., *Mechanics Research Communications*, **5** (1978), pp.375-381.
20. Muskhelishvili, N. I., *Singular Integral Equations (J. M. Radok, Trans.)* (1953), N. V. P. Noordhoff, Groningen, Holland.
21. Bilby, B. A. and Eshelby, J. D., *Fracture, An Advanced Treatise* (1968), Liebowitz, H. (Ed), Vol. I, pp.134-137.
22. Neuber, H., *Kerbspannungslehre* (1958), 2nd ed., p.84, Springer-Verlag, Berlin.